Collective Chaos in a Population of Globally Coupled Oscillators

Article *in* Progress of Theoretical Physics · February 1993

DOI: 10.1143/PTP.89.313

CITATIONS
170

READS
412

2 authors, including:

Naoko Nakagawa
Ibaraki University
76 PUBLICATIONS **1,590** CITATIONS

SEE PROFILE

Progress of Theoretical Physics, Vol. 89, No. 2, February 1993

Collective Chaos in a Population of Globally Coupled Oscillators

Naoko NAKAGAWA and Yoshiki KURAMOTO

Department of Physics, Kyoto University, Kyoto 606-01

(Received October 5, 1992)

Different forms of collective chaos are found in a large population of globally coupled identical oscillators of the complex Ginzburg-Landau type. Under certain conditions, the entire population splits into three point-clusters, and their coupled dynamics generates chaos of low dimension. It also occurs that all these clusters are fused into one continuous distribution in the form of a closed loop. This object exhibits stretching-and-folding behavior characteristic to chaos, whose interpretation is provided from the approximate equivalence of our system to an ensemble of independent oscillators driven by a common periodic field. It is found that collective chaos also arises when fused and point clusters coexist.

§ 1. Introduction

Large populations of globally coupled limit-cycle oscillators provide a unique class of nonlinear systems of considerable current interest.[1)~16)] Such systems are in some sense intermediate between low-dimensional dynamical systems and spatially extended systems. This is because, while the degrees of freedom involved may be very large as in extended systems, globally coupled oscillators can also be looked upon as a simple assembly of mutually independent oscillators except that they are under a common driving force. Thus, it is natural to expect that the chaotic dynamics in such systems will also show some mixed characters between low-dimensional chaos and spatio-temporal chaos. The present study seems to support our anticipation at least partially.

Recent studies based on the phase model revealed[13),15)] that globally coupled oscillators reorganize themselves into a number of subpopulations in each of which the oscillators behave identically. This is called *clustering*, while similar behavior in globally coupled chaotic maps was discovered earlier by Kaneko.[17)] In oscillator systems, various modes of clustering are possible[13),15)] which result in a considerable variety in oscillation pattern of collective variables. Within the framework of the phase model, however, no chaotic dynamics at the collective level seems possible. Once the amplitude degree of freedom is taken into account, in contrast, collective chaos occurs quite easily. This was first demonstrated numerically by Matthews, Mirollo and Strogatz[11)] for the real-coefficient Ginzburg-Landau oscillators with frequency distribution. More recently, Hakim and Rappel[18)] (referred to as I hereafter) studied globally coupled complex Ginzburg-Landau oscillators *without* frequency distribution or any other randomness, i.e.,

$$\dot{W}_j = W_j + K(1+ic_1)(\bar{W} - W_j) - (1+ic_2)|W_j|^2 W_j\,, \quad (j=1, 2, \cdots N)$$

$$\bar{W} = \frac{1}{N}\sum_{k=1}^{N} W_k\,, \tag{1·1}$$

and discovered collective chaos as well as clustering. In the present paper, we will also be concerned with the above model, and report a number of additional results from our own analysis which has been carried out independently. In the following sections, we start with some cosideration of the weak-coupling limit of Eq. (1·1), and proceed to the stability argument of two trivial collective states. Then we study clustering states in some detail, and discuss the sequence of bifurcations leading to collective chaos. It is argued that different forms of collective chaos occur depending on parameter values. In one case, chaos arises from the coupled dynamics among three point-clusters. In another case, all the clusters have already been fused to form a continuous distribution in the complex W-plane. Thus the collective chaos of this type should be associated with the complex motion of the distribution rather than the "microscopic" dynamics of the individual oscillators. Instantaneous distribution in the W-plane looks very much like a Poincaré section for a periodically forced oscillator. Moreover, a series of snapshots of the oscillator distribution show that the distribution repeats stretching and folding, which is as if we are looking at a series of Poincaré sections taken at different phases of a collapsed torus. A simple interpretation will be given for such peculiar behavior of the distribution. We also find a little different type of chaos with ρ-shaped distribution, which is the one discovered by Hakim and Rappel[18] with a qualitative interpretation of its origin.

§ 2. Relation to the phase model and the stability of some trivial collective states

Equation (1·1) includes three parameters K, c_1 and c_2. For searching a suitable parameter domain in which complex collective dynamics is expected, it is helpful to consider the weak-coupling limit of Eq. (1·1). When K is sufficiently small, Eq. (1·1) is reduced to the phase model[5] of the form

$$\dot{\phi}_j=\omega+\frac{K}{N}\sum_k \sin(\phi_k-\phi_j+\phi_0)\,, \tag{2·1}$$

where ϕ_j is the phase of W_j, and

$$\omega=-c_2\,,$$

$$\cos\phi_0=1+c_1c_2\,. \tag{2·2}$$

Thus the coupling is attractive (i.e., the phase difference $\Delta\phi$ between an isolated pair of oscillators tends to vanish) if $|\phi_0|<\pi/2$, while it is repulsive (i.e., $\Delta\phi$ tends to π) if $|\phi_0|>\pi/2$. In the case of attractive coupling, all ϕ_j will become identical to form a single point-cluster oscillating with frequency $\omega+K\sin\phi_0$. That is,

$$\phi_1=\phi_2=\cdots=\phi_N=(\omega+K\sin\phi_0)t\,. \tag{2·3}$$

We call the above the 1-cluster state. In the case of repulsive coupling, the 1-cluster state is no longer stable. The oscillators will then be strongly frustrated and unable to find a stable phase configuration until the self-consistent internal field $\bar{W}$ is completely canceled. Thus, any phase distribution of the form $f(\phi+\omega t)(=f(\phi+\omega t+2\pi))$ should remain stable, once established, provided that it is free from the first

Fourier component (i.e., $\int_0^{2\pi} f(\phi) \times \exp(i\psi) d\psi = 0$). All ϕ_j then rotate freely, for which we call the *incoherent state.* Of particular importance among various phase distributions in the incoherent state is the uniform distribution

$$f(\phi) = (2\pi)^{-1}, \qquad (2\cdot4)$$

because any nonuniform components of f would decay on introducing infinitesimal noise, frequency distribution or other randomness.[5] In any case, the phase diagram is extremely simple in the weak coupling limit; the oscillators are either perfectly synchronized or completely independent. The transition between these states occurs at $1+c_1c_2=0$. No complex behavior such as clustering and chaos can occur. Note that clustering does occur even within the phase model if the coupling function or the free dynamics of the individual oscillators is changed from the form in Eq. (2·1).[13),15)] However, the origin of clustering discussed below is different because it comes from amplitude effects. When the coupling strength K becomes finite, Eq. (1·1) still admits the two trivial collective states mentioned above. However, the stability limits of these states no longer coincide. In what follows, the parameter region where the 1-cluster state is linearly stable will be called region A, and for the incoherent state region B. Since the stability boundary of A and that of B no longer coincide, the third, nontrivial dynamical regime which we denote C should appear in between. Figure 1 shows the stability diagram in the c_1-K plane which is essentially the same as that obtained analytically in I. The lines L_A and L_B give the stability limits of the 1-cluster state and the uniform incoherent state, respectively. Linear stability analysis shows that as we cross L_A, $N-1$ eigenvalues become zero simultaneously. When crossing L_B, in contrast, a pair of eigenvalues become pure imaginary. However, the latter is not the usual Hopf bifurcation because there are still infinitely many neutral modes as understood from the previous arguments on the phase model. The analytic forms of L_A and L_B are given by

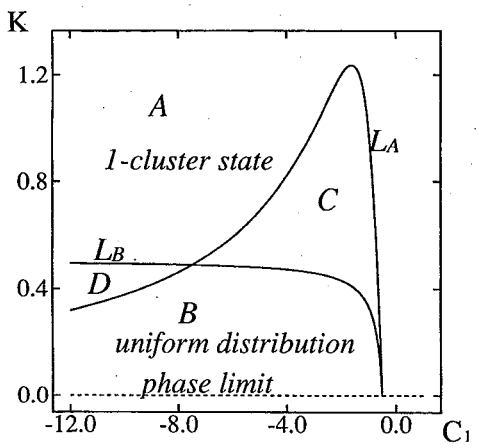

Fig. 1. Stability diagram in the c_1-K plane, where c_2 is fixed at 2.0. L_A and L_B divide the plane into four characteristic regimes. They are: A (1-cluster state stable), B (uniform phase distribution stable), C (both unstable) and D (both stable). The phase model becomes asymptotically valid as the broken line $K=0$ is approached.

$$(1+c_1^2)K+2(1+c_1c_2)=0 \qquad (2\cdot5)$$

for L_A, and

$$K(2K-1)c_1^2+4(K-1)(2K-1)c_1c_2-K(K-1)c_2^2+(3K-2)^2=0 \qquad (2\cdot6)$$

for L_B. These lines converge into a single line $1+c_1c_2=0$ as K approaches 0. Our main concern in the subsequent sections will be region C where neither the 1-cluster

state nor the uniform incoherent state is stable. Note also that we have a region (region D) in which these trivial states are both stable.

There are a few comments to be made on the stability analysis of the incoherent state. Hakim and Rappel[18] employed the standard method by linearizing Eq. (1·1) around an incoherent state of the form $W_j=\sqrt{1-K}\exp(-i(Kc_1+(1-K)c_2)t+i\psi_j)$ with the constraint $\bar{W}=0$. It seems, however, that a little different approach as we describe below is more suitable for clarifying what is implied physically by the destabilization of the incoherent state. For the sake of simplicity, we restrict ourselves to the stability of the uniform incoherent state, i.e., uniform phase distribution on the circle of radius $\sqrt{1-K}$ in the W-plane. We expect that the instability is caused by a nonuniform fluctuation in the phase distribution f coupled with a small distortion of the closed loop on which the oscillators are to be distributed. This naturally leads to the idea that we work with the phase distribution $f(\psi, t)$ and the "shape function" $r(\psi, t)$ rather than with the individual oscillator variables W_j. It is easy to change the representation of the dynamical equations from the $W_j(t)$'s to $f(\psi, t)$ and $r(\psi, t)$. By linearizing the equations for f and r around $f=(2\pi)^{-1}$ and $r=\sqrt{1-K}$, and solving for the eigenvalues, we obtain the critical condition (2·6). From the fact that the critical eigenmodes are associated with the fundamental Fourier components of f and r, what is implied by the instability will intuitively be clear.

In presenting our numerical results in the subsequent two sections, it is convenient to work with the coordinate system in which the phase of the complex mean field $\bar{W}(t)$ looks constant. We now put

$$\bar{W}=R\exp(i\theta)\,, \tag{2·7}$$

$$W_j=Z_j\exp(i\theta)\,. \tag{2·8}$$

Then the equation in the new frame is expressed as

$$\dot{Z}_j=(1-i\Omega(t))Z_j+K(1+ic_1)(R(t)-Z_j)-(1+ic_2)|Z_j|^2Z_j\,, \tag{2·9}$$

where

$$\Omega=\dot{\theta} \tag{2·10}$$

and

$$R=\frac{1}{N}\sum_j Z_j\,. \tag{2·11}$$

Thus the 1-cluster state is represented by the fixed point

$$Z_j=1\,. \quad (j=1, 2, \cdots N) \tag{2·12}$$

Further, if $\bar{W}$ changes quasiperiodically, while R and Ω being simply periodic, then each oscillator in the new frame will be under a periodic forcing by the mean field. In what follows, when we use the terms like "periodic" and "quasi-periodic" for collective or individual motions, they should be understood as referring to the behavior in the new frame.

In I, a basic equation with slightly different form from Eq. (1·1) was used. That is,

$$\dot{W}_j=\mu W_j+(1+i\beta)(\bar{W}-W_j)-(1+i\alpha)|W_j|^2 W_j\,. \tag{2·13}$$

The two equations are obviously equivalnt with the identifications

$$\mu=K^{-1}\,,\quad \beta=c_1\,,\quad \alpha=c_2\,. \tag{2·14}$$

§ 3. Clustering and the first type of collective chaos

We now investigate the dynamics near the line L_A by numerically integrating Eq. (1·1). We fixed the parameters c_1 and c_2 as $c_1=-1.0$ and $c_2=2.0$, and decreased K. The population size assumed is typically $N=800$, while a smaller system with $N=100$ was used when elaborate calculations were needed such as in producing the results in Figs. 2 and 3. We employed the Runge-Kutta method typically with the time step of 0.01. Whenever the stability of the n-cluster state is clear from the simulation for the full population, we worked for some purposes with a reduced form of Eq. (1·1) to n coupled oscillator equations taking account of empirically determined cluster sizes.

Our numerical calculation shows that the instability of the 1-cluster state occurs at $K=K_1(=1.0)$, leading immediately to a 2-cluster state of the form

$$Z_1=Z_2=\cdots=Z_{N_1}\equiv Z^{(1)}\,,$$
$$Z_{N_1+1}=Z_{N_1+2}=\cdots=Z_N\equiv Z^{(2)}\,, \tag{3·1}$$

where $Z^{(1)}$ and $Z^{(2)}$ are constants and the distance $|Z^{(1)}-Z^{(2)}|$ is finite from the outset. Since the critical zero

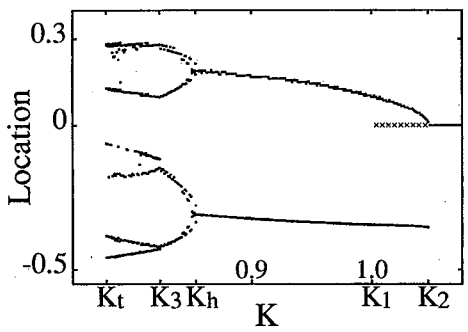

Fig. 2. Locations of the clusters. Imaginary part of Z_j as a function of the coupling strength K is shown for each cluster. Above K_2, 1-cluster state is the only stable state. Between K_1 and K_2, 1- and 2-cluster states coexist, where the metastable 1-cluster branch is indicated with crosses. 2-cluster state persists down to K_h where the clusters start to oscillate. Pitchfork type branches in the figure indicate the maxima and minima of $\mathrm{Im}Z_j$ during oscillation, and not the doubling in the number of the clusters. 3-cluster state starts at K_3 and persists down to K_t where the second oscillatory instability occurs.

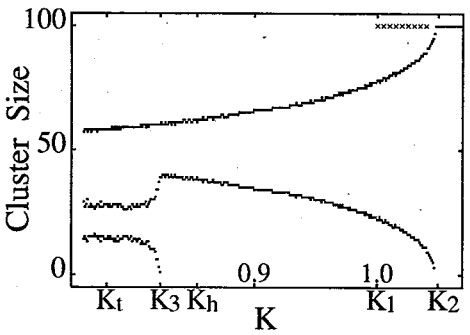

Fig. 3. Normalized cluster sizes p_j as a function of the coupling strength K. The meanings of K_1, K_2, K_3, K_h and K_t are the same as in Fig. 2. Note that as K_2 is approached from below, the size of the smaller cluster tends to vanish. The same is true as K_3 is approached from below.

eigenvalues turn out to be $(N-1)$-fold degenerate on account of the global nature of the coupling, usual bifurcation analysis does not seem to apply for predicting what collective states are realized beyond criticality. In the 2-cluster state, the normalized sizes of the clusters, i.e., $p_1=N_1/N$ and $p_2=1-p_1$ depend on initial condition as well as on K. In most of our numerical simulations, we initially distributed the oscillators on the unit circle in the complex W-plane. In Figs. 2 and 3 we respectively show how the locations of the clusters (actually $\mathrm{Im}Z_j$) and their normalized sizes p_j change with K. As we noted, the transition between the 1- and 2-cluster states is discontinuous, and they coexist in the parameter range $K_1<K<K_2$ ($\simeq 1.05$). It is interesting to see that the size of one of the clusters tends to zero as the stability limit K_2 of the 2-cluster state is approached.

On decreasing K below K_1, the stationary 2-cluster state becomes oscillatory unstable, which occurs at K_h. Then $Z^{(1)}$ and $Z^{(2)}$ start small-amplitude oscillations with finite frequency, implying Hopf bifurcation. In Fig. 2, this is indicated by a pitchfork bifurcation diagram in each cluster; the upper and lower branches simply show the maxima and minima of the amplitude of the cluster oscillations, and they should never be confused with "cluster-doubling". On further decreasing K down to K_3, the smaller cluster splits into two, one of which starting with infinitesimal size. Thus we have three point-clusters. At first, they are still time-periodic, but this seems to be followed by the second oscillatory instability. The structure of the subsequent bifurcations leading to chaos is not clear from our numerical simulation using a large N system, because they occur in a very narrow range of K. Since we confirmed that the three point-clusters are preserved at least up to the onset of chaos, more details on the transition were analyzed by working with the three-oscillator reduction of Eq. (1·1) mentioned earlier. By examining the Poincaré section of the orbit of one of the clusters, it was then found that after the second oscillatory instability, phase locking into period 37 occurs. The corresponding Poincaré section is shown in Fig. 4. This

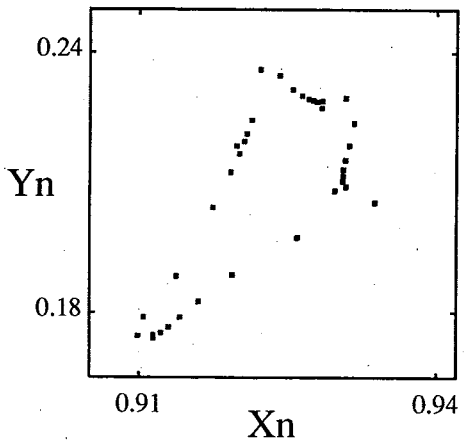

Fig. 4. Poincaré section for the 3-cluster state at $K=0.7725$. The dots show the values of $Z=(X, Y)$ of one of the clusters taken each time the orbit in the 3×2-dimensional phase space crosses a certain plane in a prescribed direction.

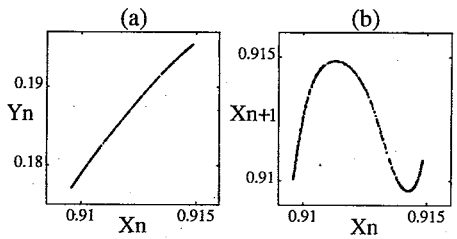

Fig. 5. (a) Poincaré section for the chaotic 3-cluster state at $K=0.7720$. The line segment indicated is the island which has developed from one of the 37 periodic points in Fig. 4 through repeated period-doubling bifurcations. Note that its one-dimensionality is almost complete. (b) Corresponding one-dimensional return map.

locking state soon loses stability against a series of period-doubling bifurcations. For $K=0.772$ where the system seems to be already chaotic, a Poincaré section taken at every 37 periods forms a thin line. The corresponding return map for ReZ gives a typical form of a chaotic one-dimensional map. There results are illustrated in Figs. 5(a) and (b).

§ 4. Cluster fusion and the second type of collective chaos

The chaotic behavior of the three point-clusters as we discussed in the preceding section can only be seen in a fairly limited range of K. Beyond this range, two of the clusters can no longer remain to be a point cluster, but they are fused to form a continuous distribution on a string as shown in Fig. 6. Thus the effective degrees of freedom suddenly jump up to $O(N)$. The nature of chaos in such a situation is not clear yet (but see the last paragraph of this section).

We changed the parameter values of c_1 and c_2 as well as K, in order to find different types of chaos which are easier to interpret. Figure 7 shows a series of snapshots of the distribution where no point-cluster is seen. The assumed parameter values, i.e., $c_1=-2.0$, $c_2=3.0$ and $K=0.5$ imply that we are relatively close to the critical line of the uniform incoherent state. The entire population now forms a single continuous distribution in a closed loop. It is remarkable that it looks much like the Poincaré sections for a periodically driven oscillator observed at different phases of the driving force. The distribution shows a typical stretching-and-folding structure characteristic to chaos, implying that the distance between a pair of nearby oscillators grows exponentially in time. As expected, the blowup of a small part of the distribution reveals a layered fine

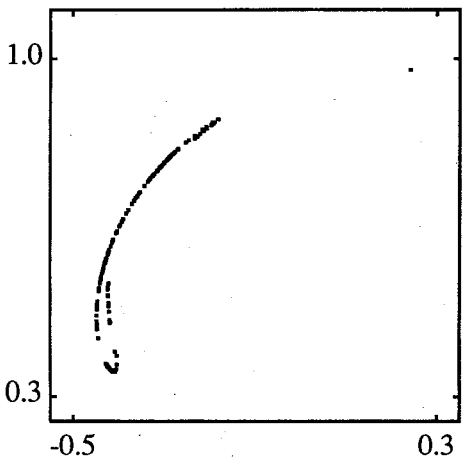

Fig. 6. Snapshot of the distribution of 800 oscillators in the complex plane, where $c_1=-1.0$, $c_2=2.0$ and $K=0.75$. Two of the clusters are now fused to form a string.

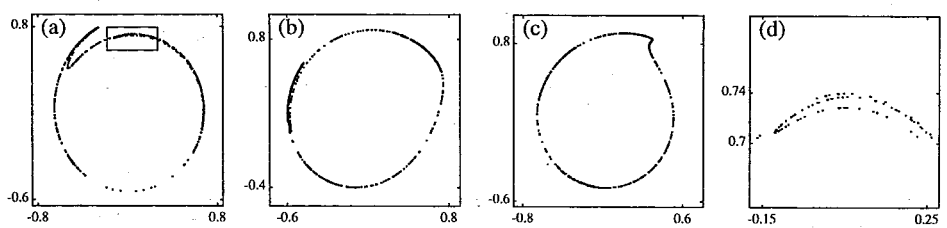

Fig. 7. (a)~(c) Three successive snapshots of the distribution of 800 oscillators in the complex plain, where $c_1=-2.0$, $c_2=3.0$ and $K=0.5$. The distribution repeats stretching-and-folding motions, but its periodicity is only approximate. (d) Blowup of a small part of the distribution enclosed by a square in (a), showing a layered fine structure.

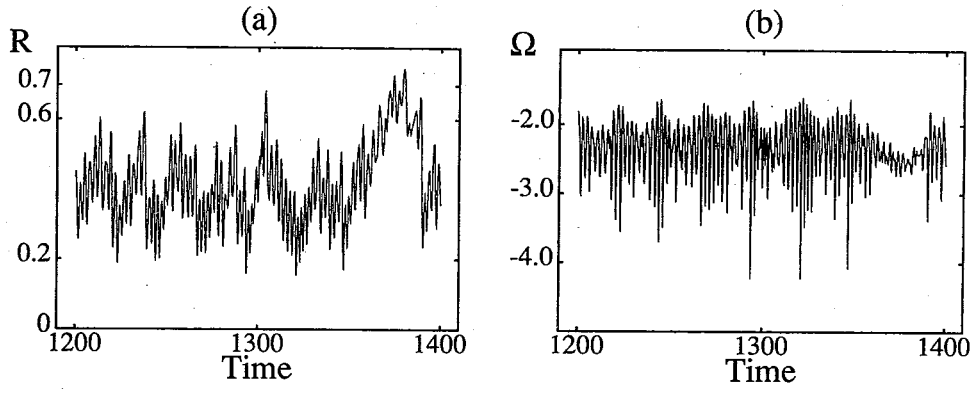

Fig. 8. Collective behavior corresponding to Fig. 7. (a) Amplitude R of the mean fied versus time; (b) Instantaneous frequency Ω of the mean field versus time.

structure. The collective behavior under the same condition is displayed in Fig. 8. We see that the amplitude R and the instantaneous frequency Ω of the mean field varies rather irregularly, still the existence of a periodic component is suggested. For comparison's sake, we show in Fig. 9 a snapshot of the distribution for a slightly different K value. Then no stretching-and-folding structure seems to exist. This was confirmed from a number of snapshots wihch are not shown in the figure. Thus, there is no orbital instability at the "microscopic" level. The corresponding collective behavior given in Fig. 10 shows much more apparent periodicity than in Fig. 8. Still some chaotic fluctuations persist in spite of the absence of microscopic chaos.

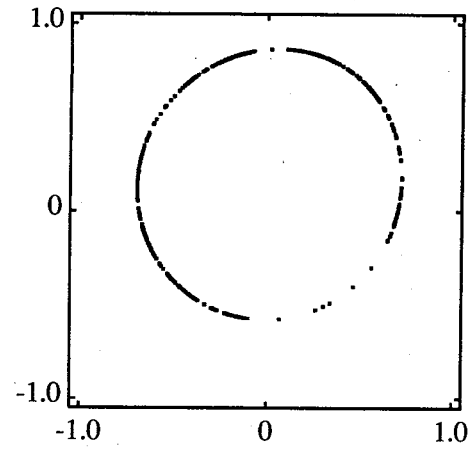

Fig. 9. Snapshot of the distribution of 800 oscillators in the complex plain. c_1 and c_2 are the same as in Fig. 7, but K is smaller, i.e., $K=0.45$. From a series of snapshots (not shown here), no indication of stretching-and-folding structure is obtained.

Distribution patterns as displayed in Figs. 7 and 9 can be understood from Eq. (2·9) by assuming R and Ω to be strictly periodic. We replaced these quantities with piecewise-parabolic functions which approximate the empirical oscillation patterns in Fig. 10 (see Fig. 11). Equation (2·9) is now looked upon as describing a periodically forced oscillator. Figure 12 shows some results of its numerical simulation. By tuning the parameters, especially the oscillation amplitude R, we see that the behavior either in Fig. 7 or in Fig. 9 is reproducible. When we use different and more accurate values of I (i.e., period of R) in respective cases, there is no essential change in the results. Note that no explanation for the origin of the present type collective chaos has been provided yet, because we have simply assumed the collective variables R and Ω to be *periodic*. What has been explained is only the *individual* chaos, whereas

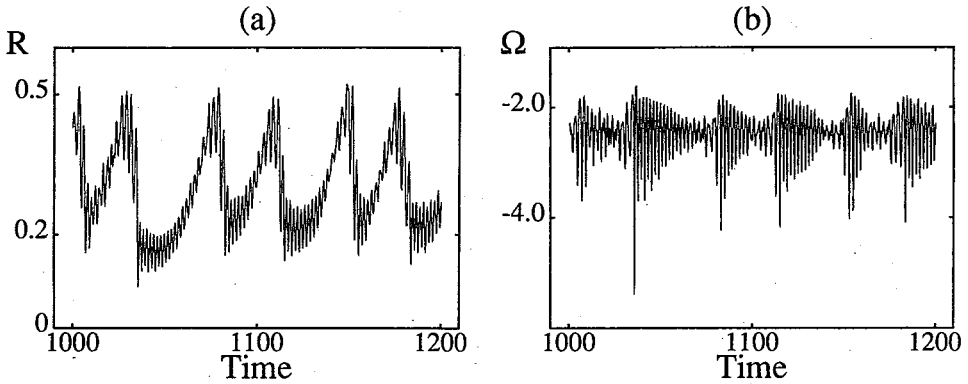

Fig. 10. Collective behavior corresponding to Fig. 9. (a) Amplitude R of the mean field versus time; (b) Instantaneuos frequency Ω of the mean field versus time. Much clearer periodicity is seen as compared to Fig. 8.

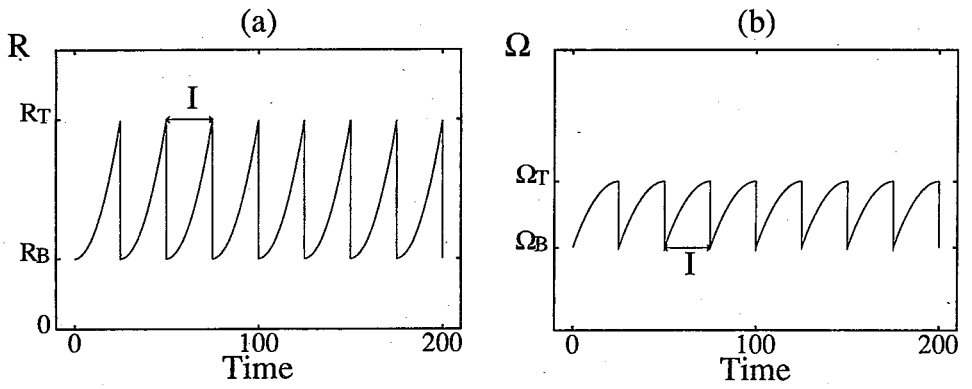

Fig. 11. Modeling the mean field behavior by piecewise-parabolic periodic functions. (a) Model for the amplitude R; (b) Model for the instantaneous frequency Ω. They include some parameters, but in producing the results of Fig. 12, the only parameter we changed is R_T, i.e., the maximum value of R.

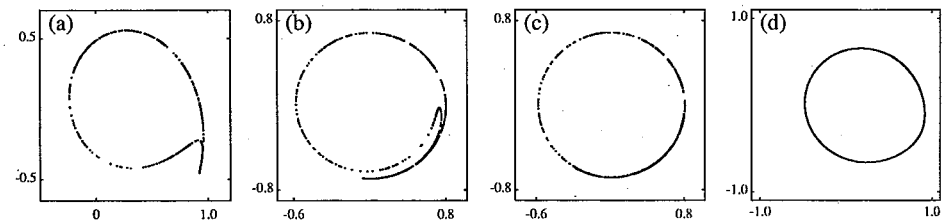

Fig. 12. Poincaré sections for one forced oscillator described by Eq. (2·9) with periodic R and Ω. (a)~(c) The sections are taken at different phases of $R(t)$. Some characteristics of the distribution as shown in Fig. 7 are reproduced. The values of c_1, c_2 and K are the same as in Fig. 7, while $R_T=0.72$, $R_B=0.20$, $\Omega_T=-2.40$, $\Omega_B=-2.60$ and $I=25.0$. (d) This figure corresponds to Fig. 9. The values of c_1, c_2 and K are the same as in Fig. 9, while $R_T=0.45$, $R_B=0.20$, $\Omega_T=-2.40$, $\Omega_B=-2.60$ and $I=25.0$.

individual chaos does not always imply collective chaos. Since R and Ω are the quantities to be determined self-consistently as functions of the distribution itself, the important question yet to be answered seems to be how the periodic self-consistent

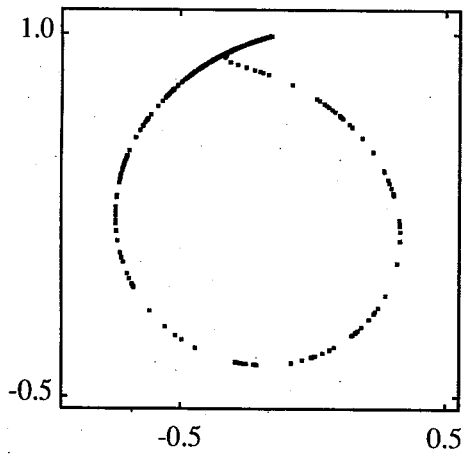

Fig. 13. Snapshot of a ρ-shaped distribution of 800 oscillators in the complex plain. Parameter values are $c_1=-1.0$, $c_2=2.0$ and $K=0.45$.

solution for R and Ω can be so unstable as to exhibit chaos.

In the preceding section, we assumed $c_1=-1.0$ and $c_2=2.0$. For these parameter values and for smaller K, fused clusters show a ρ-shaped distribution (see Fig. 13). We seem to be in the same situation as that discussed by Hakim and Rappel.[18] The corresponding mean field dynamics is shown in Fig. 14. Although the ρ-shaped distribution itself may not look much different from the distribution in Fig. 12, strong difference between the corresponding mean field behaviors is apparent, implying also the difference in the origin of chaos (collective or individual). Following I, we suppose to the zeroth approximation that R and Ω are constants whose values are to be estimated from the time-averages of their empirical data. Then it is easy to see from Eq. (2·9) (now regarded as a periodically forced one-oscillator equation) that the oscillator is locked or unlocked depending on the values of R and Ω (see Fig. 15). In particular, under fixed Ω, larger values of R favor locking and smaller values unlocking. The empirical value of R seems to be marginal between these two states. Thus the chaotic behavior may be associated with irregular transitions between them, which was pointed out by Hakim and Rappel.[18] The transitions seem to occur inevitably from a self-consistency requirement. More specifically, if the dominant part of the population comes to stay in the unlocked state, then R is increased, by which the unlocked state gives way to the locked state; if the locked state is too much populated, then the situation is reversed.

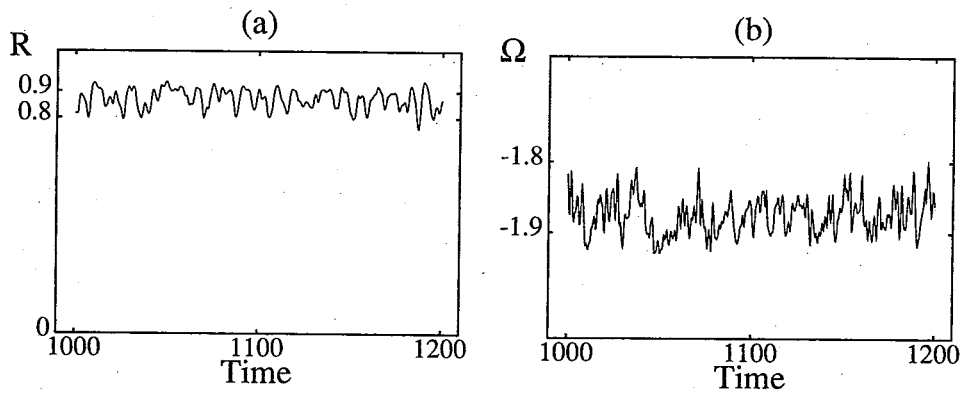

Fig. 14. Collective behavior corresponding to Fig. 13. (a) Amplitude R of the mean field versus time; (b) Instantaneous frequency Ω of the mean field versus time. Qualitative difference in oscillation pattern from those in Figs. 8 and 10 is apparent.

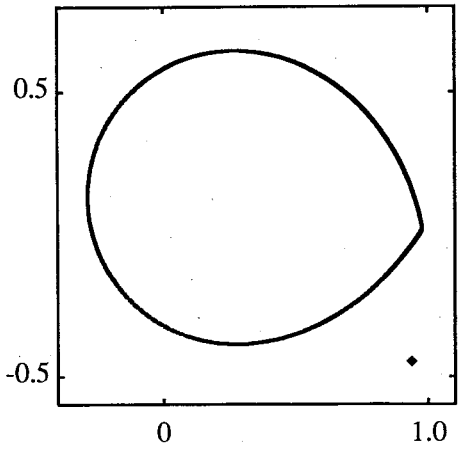

Fig. 15. Orbits of the solution of the one-oscillator equation (2·9) with constant R and Ω. Slight difference in the value of R changes the behavior drastically. For $R=0.92$, the only attractor is the fixed point indicated by a dot. For $R=0.91$, the fixed-point attractor vanishes through a saddle-node bifurcation, and the only attractor is the periodic orbit with an angular part as shown in the figure. Switching of the individual oscillators between the fixed point and the closed orbit roughly explains the distribution pattern as in Fig. 13.

§ 5. Summary

We found different types of collective chaos in globally coupled complex Ginzburg-Landau oscillators. In one case, the occurrence of chaos is preceded by spontaneous splitting of a perfectly synchronized population into two and then three point-clusters, and increasing complication of their relative motion finally leads to chaos. In the other case, the clusters are fused at least partially. In particular, when the entire population forms one continuous distribution, it behaves like a statistical ensemble for an oscillator system under periodic forcing. Actually, however, the forcing or the mean field is not periodic, and the origin of its nonperiodicity is yet to be explained from self-consistency arguments.

Acknowledgements

The present work is supported by the Japanese Grant-in-Aid for Science Research Fund from the Ministy of Education, Science and Culture (Nos. 04218109 and 04231107).

References

1) A. T. Winfree, J. Theor. Biol. **16** (1967), 15.
2) Y. Kuramoto, in *International Symposium on Mathematical Problems in Theoretical Physics*, H. Araki ed., Lecture Notes in Physics **39** (Springer, New York 1975), p. 420.
3) Y. Aizawa, Prog. Theor. Phys. **56** (1976), 703.
4) Y. Yamaguchi, K. Kometani and H. Shimizu, J. Stat. Phys. **26** (1981), 719.
5) Y. Kuramoto, *Chemical Oscillations, Waves, and Turbulence* (Springer, Berlin 1984).
6) G. B. Ermentrout, J. Math. Biol. **22** (1985), 1.
7) H. Daido, Prog. Theor. Phys. **77** (1987), 622.
8) Y. Kuramoto and I. Nishikawa, J. Stat. Phys. **49** (1987), 569.
9) H. Sakaguchi, S. Shinomoto and Y. Kuramoto, Prog. Theor. Phys. **79** (1988), 600.
10) G. B. Ermentrout, Physica **D41** (1990), 219.
11) P. C. Matthews, R. E. Mirollo and S. H. Strogatz, Physica **D52** (1991), 293.
12) S. H. Strogatz and R. E. Mirollo, J. Stat. Phys. **63** (1991), 613.
13) D. Golomb, D. Hansel, B. Shraiman and H. Sompolinsky, Phys. Rev. **A45** (1992), 3516.
14) Y. Kuramoto, Physica **D50** (1991), 15.
15) K. Okuda, Physica **D**, to appear.
16) S. H. Strogatz, R. E. Mirollo and P. C. Matthews, Phys. Rev. Lett. **68** (1992), 2730.
17) K. Kaneko, Physica **D41** (1990), 137; **D54** (1991), 5.
18) V. Hakim and W. J. Rappel, Phys. Rev. **E**, to appear.